International Journal of Engineering Inventions
e-ISSN: 2278-7461, p-ISSN: 2319-6491
Volume 14, Issue 12 [December 2025] PP: 73-82

Removal and Recovery of Cu (II) and Cr (VI) from Metal Industry Wastewater Using Nanocomposite

Sevil AKÇAĞLAR
Department of Mechanical Engineering, Faculty of Engineering, Dokuz Eylül University, İzmir, Turkey,
Corresponding Author: sevil.akcaglar@deu.edu.tr

ABSTRACT: *In this study, we present a simple and effective two-step process combining adsorption and photoreduction for the removal, separation, and recovery of Cu(II) and Cr(VI) from mixed heavy-metal wastewater. First, a TiO_2–ZrO_2 solid-solution photocatalyst was applied to reduce Cr(VI) in the absence of a sacrificial agent, achieving a removal efficiency of 95%, while Cu(II) remained predominantly in the aqueous phase. Second, a commercial cation-exchange resin (Lewatit TP207) was used to selectively adsorb Cu(II) without significantly altering Cr(VI) concentrations. When these processes were combined—regardless of the sequence—both Cu(II) and Cr(VI) were reduced to levels meeting typical discharge standards. The most effective treatment sequence was found to be ion exchange followed by photocatalysis: residual Cu(II) was reduced to 0.06 mg L^{-1}, and total Cr (with no detectable Cr(VI)) was 0.74 mg L^{-1}. The separation factor for Cu(II)/Cr(VI) reached 11,949, with recovery efficiencies of 99.17 % for Cu(II) and 96.29 % for Cr(VI). This work demonstrates a promising dual-process strategy for the selective removal and recovery of heavy metals in complex wastewater streams.*

Keywords: *TiO_2–ZrO_2 nanocomposite, Cu(II), Cr(VI), adsorption, photoreduction, waste-water treatment*

Date of Submission: 12-12-2025 Date of acceptance: 24-12-2025

I. INTRODUCTION

Acidic heavy metal–containing wastewater is commonly generated by modern industries and requires treatment to prevent environmental contamination [1]. These toxic metal ions are also valuable resources and can be recovered. Cu/Cr wastewater, typically produced by the electroplatin electroplating industry, is conventionally treated using chemical precipitation [2], electrochemical methods [3], ion exchange [4], photocatalysis [5,6], and adsorption [7,8]. Efficient removal and separation of Cu and Cr ions is important for both environmental protection and resource recovery.

Simultaneous removal and separation of Cu and Cr in a single process remains challenging, despite some studies reporting partial success [9–11]. For instance, ion exchange resins removed 96% of Cu and 68% of Cr from chromated copper arsenate [9], yet the treated water and metal separation did not meet regulatory standards. Therefore, improving the efficiency of Cu/Cr removal and separation remains a critical challenge for traditional adsorbents.

Photocatalysis offers a promising alternative, enabling the reduction of toxic metal ions into less harmful or insoluble forms, such as Cr(VI) to Cr(III) or Cu(II) to Cu(0) [5,12]. The metals produced can then be recovered via precipitation or adsorption, facilitating resource recycling [13,14]. Photoreduction can achieve discharge standards for Cr(VI) (0.5 mg/L), total Cr (1.5 mg/L), and total Cu (0.5 mg/L), highlighting its potential for environmental protection [15].

However, the practical application of photoreduction for Cu/Cr wastewater faces two main limitations: the need for external sacrificial reagents to consume photo-generated holes, and the simultaneous, non-selective deposition of Cu and Cr. Overuse of sacrificial reagents can lead to secondary pollution [16], while non-selective deposition requires additional steps to separate Cu and Cr for recovery. Selective reduction of one metal ion without additives, followed by a simple process to recover the other, would enable complete wastewater purification and is attractive for industrial applications.

ZrO_2, a wide-bandgap photocatalyst, can directly photoreduce Cr(VI) to insoluble species under UV light [17], but it cannot reduce Cu(II), offering a pathway for selective Cr(VI) removal, albeit with low light utilization. TiO_2 has a narrower bandgap, yet the sequential separation of Cr and Cu remains necessary, increasing treatment costs. Additionally, both systems require sacrificial reagents, introducing secondary treatment steps. Therefore, developing a photocatalytic process without organic scavengers is highly desirable for Cu/Cr hybrid wastewater treatment.

A scavenger-free photoreduction strategy has been demonstrated for metals such as Ag, Ru, Au, Rh, Pt, and Cr using water as the sacrificial reagent [18–22]. Incorporating TiO_2 into ZrO_2 enables a similar

scavenger-free photoreduction of Cr(VI) to insoluble Cr species. In such a system, Cr and Cu can be effectively separated: only Cr(VI) is photoreduced, while residual Cu(II) can be recovered using conventional methods. A Ti/Zr solid solution thus presents a promising photocatalyst for the selective removal of Cr(VI), and a weakly acidic macroporous cation-exchange resin, Lewatit TP207, can be employed to remove Cu(II).

In this study, a TiO_2–ZrO_2 solid solution was synthesized and applied in a sacrificial reagent-free photoreduction process for Cr(VI) removal, while TP207 was used to remove the remaining Cu(II). The selective removal efficiency and adsorption dynamics of Cr(VI) and Cu(II) were systematically investigated. Various coupled treatment sequences combining these two processes were evaluated to determine the optimal strategy for selective removal and recovery of Cr and Cu from acidic wastewater.

II. MATERIALS AND METHODS

2.1. Materials

The photocatalyst was prepared using isopropanol, n-butyl titanate, zirconium butoxide, and cetyltrimethylammonium bromide (CTAB). Potassium dichromate ($K_2Cr_2O_7$), copper sulfate pentahydrate ($CuSO_4 \cdot 5H_2O$), and nitric acid (HNO_3) were obtained from Chengdu Kelong Reagent Co., Ltd. All chemicals were used as received without further purification. Lewatit TP207 ion exchange resin was procured from Shenzhen Yijiayuan Environmental Protection Technology Co., Ltd. (Table 1).

Table (1). Basic characteristics of Lewatit TP207 ion exchange resin [4].

Property	**Value**
Matrix	PS–DVB macroporous
Functional groups	CH2N(CH2COOH)2
Total exchange capacity (meq/g)	2.2
pH range	0–14
Maximum operating temperature (K)	313
Bulk density (g/dm³)	720

2.2. Preparation of the photocatalyst and simulated wastewater

The photocatalyst was prepared according to the following procedure [12]. A solution containing 40 mL of isopropanol, X mL of n-butyl titanate, Y mL of zirconium butoxide, and an appropriate amount of CTAB was prepared and denoted as solution A (X + Y = 10 mL). Subsequently, an aqueous 10 vol% isopropanol solution was added dropwise to solution A under continuous stirring. After 4 h of reaction, the resulting gel was washed with deionized water, dried, and calcined at Z °C for 4 h to obtain TiO_2–ZrO_2, designated as TiX ZrY(Z).

Simulated wastewater samples were prepared to contain Cr(VI) (20 mg/L), Cu(II) (20 mg/L), and a mixed Cr(VI)/Cu(II) system (40 mg/L total, Cu:Cr = 1:1). Potassium dichromate ($K_2Cr_2O_7$) and copper(II) sulfate pentahydrate ($CuSO_4 \cdot 5H_2O$) were used as the sources of Cr(VI) and Cu(II), respectively. The pH of all solutions was adjusted to 3 using 0.1 M HNO_3.

Photocatalytic experiments were conducted as follows. A total of 20 mL of simulated wastewater and 0.02 g of the photocatalyst were added to a quartz reaction tube, which was subsequently placed in a photoreactor (CEL-LAB500, Zhongjiajinyuan, Beijing, China). After reaching adsorption–desorption equilibrium under dark conditions, the photoreduction experiments were performed under UV irradiation using a 500 W lamp.

Following photocatalysis, the residual concentration of Cr(VI) in the solution was determined using a Shimadzu UV-1500PC ultraviolet–visible (UV–vis) spectrophotometer [17]. The residual concentrations of total Cr and Cu were further analyzed by inductively coupled plasma optical emission spectrometry (ICP-OES, Thermo Fisher Scientific, iCAP 7400, USA).

2.3. Ion exchange process

For the batch ion exchange experiments, 20 mL of simulated wastewater and an appropriate amount of ion exchange resin were placed in a quartz tube under continuous stirring. After the adsorption process reached equilibrium, the residual concentrations of Cr and Cu were determined using inductively coupled plasma optical emission spectrometry (ICP-OES). The adsorption capacity was calculated according to the procedure reported in the literature [4] (see Supporting Information).

Column experiments using the TP207 resin were performed to obtain the breakthrough curve. A glass column (inner diameter: 7 mm) was packed with 1.8 g of the adsorbent, and the simulated wastewater was introduced from the top at a flow rate of 8.0 mL min^{-1}. The Cu concentration in the effluent was analyzed using atomic absorption spectroscopy (AAS, AA32DCRT/GA3201).

2.4. Characterization OF TiO_2-ZrO_2 NANOCOMPOSITE

The microstructure of the photocatalyst was examined using scanning electron microscopy (SEM, HITACHI Regulus 8230, Japan). The elemental distribution on the catalyst surface was analyzed by energy-dispersive X-ray spectroscopy (EDS) and scanning transmission electron microscopy (STEM, HAADF mode) mapping using a ZEISS Libra 200FE transmission electron microscope. The crystalline structure of the catalyst was characterized by X-ray diffraction (XRD, Dandong Haoyuan DX-2700, China).

The optical absorption properties of the photocatalyst were determined using UV–vis diffuse reflectance spectroscopy (UV–vis DRS, PerkinElmer Lambda 750S, USA). Electron spin resonance (ESR) measurements were performed on a JEOL JES-FA200 spectrometer, employing 5,5-dimethyl-1-pyrroline N-oxide (DMPO) as the spin-trapping agent for hydroxyl radicals (•OH).

III. RESULTS AND DISCUSSION

3.1. Photocatalytic performance of TiO_2–ZrO_2

Following an optimization study, $Ti_{0.95}Zr_{0.05}(300)$ was selected as the optimal photocatalyst and employed for the photoreduction of Cr(VI) and Cu(II) in the absence of any scavenger reagents. As shown in Fig. 1, approximately 40% of Cr(VI) was removed from the Cr(VI) solution during the dark adsorption stage after reaching adsorption–desorption equilibrium. The concurrent decrease in total Cr concentration indicates the direct adsorption of Cr(VI) onto $Ti_{0.95}Zr_{0.05}(300)$.

Upon UV illumination, the concentration of Cr(VI) continued to decrease, reaching its minimum value of 0.44 mg L^{-1} after 2 h. Meanwhile, the total Cr concentration also declined (0.84 mg L^{-1}), although it remained slightly higher than the Cr(VI) concentration, suggesting the presence of small amounts of soluble Cr species. The treated effluent satisfied the wastewater discharge limits for both Cr(VI) (0.5 mg L^{-1}) and total Cr (1.5 mg L^{-1}).

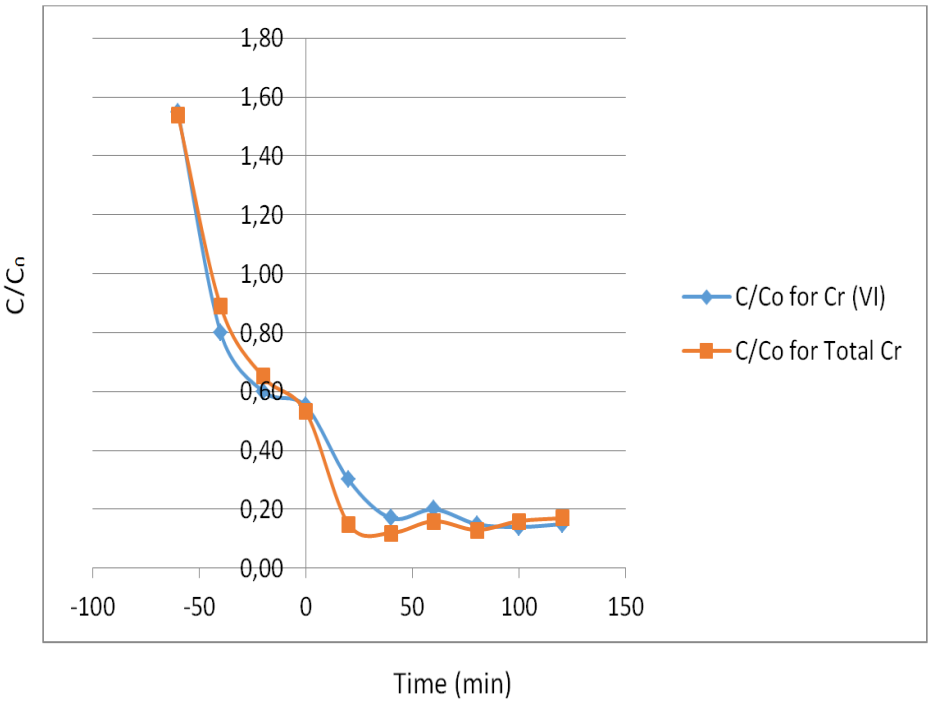

Fig. 1. Photocatalytic performance of $Ti_{0.95}Zr_{0.05}$ (300) at a catalyst concentration of 1 g L^{-1} for the treatment of a pure Cr(VI) solution. Experimental conditions: simulated wastewater volume, 20 mL; no scavenger reagent added; photocatalyst dosage, 0.02 g.

Upon introducing Cu(II) into the pure Cr(VI) solution, no significant change was observed under either dark or illuminated conditions, indicating that $Ti_{0.95}Zr_{0.05}$(300) alone could not photoreduce Cu(II) without a scavenger reagent

The dark adsorption of Cr(VI) decreased from 40% to approximately 25%, and the complete photoreduction time increased 100 min. Nevertheless, the final Cr(VI) (0.34 mg L^{-1}) and total Cr (0.76 mg L^{-1}) concentrations still met discharge standards.

For comparison, commercial P25 required 10 h of illumination to achieve similar Cr(VI) removal (0.2 mg L^{-1}) in the mixed solution, while after 3 h, the residual Cr(VI) and total Cr concentrations remained at 5.8 and 6.8 mg L^{-1}, respectively. Cu(II) remained inactive during the photoreduction process, serving only to suppress Cr(VI) adsorption and slow the overall reduction rate. The apparent kinetic constant (k) decreased from 0.0163 min^{-1} (pure solution) to 0.0066 min^{-1} in the hybrid system (Fig. 1).

In summary, $Ti_{0.95}Zr_{0.05}$ (300) selectively adsorbed, photoreduced, and deposited Cr(VI) from the Cu(II)/Cr(VI) mixed solution, achieving complete Cr(VI) removal and selective separation without any external scavenger reagent.

3.2. Existence of Cr and Cu species on $Ti_{0.95}Zr_{0.05}$ (300) after photoreduction

The selective removal of Cr(VI) from the Cu(II)/Cr(VI) mixed solution without a scavenger reagent was confirmed; however, the mechanism of this selectivity was further examined by comparing the photocatalyst before and after photoreduction.

The morphology of $Ti_{0.95}Zr_{0.05}$ (300) remained unchanged, consisting of irregular microparticles with an average size of ~2.5 μm .STEM (HAADF) mapping (Fig. 2) revealed clear Cr signals on the photocatalyst surface, with a much higher distribution density of Cr than Cu (Fig. 2C). EDS analysis further indicated surface concentrations of 2.43% Cr and 0.02% Cu . These results confirm that $Ti_{0.95}Zr_{0.05}$(300) primarily reduced and immobilized Cr species, while the trace Cu detected likely originated from residual solution trapped within the photocatalyst particles, as its content decreased after washing .

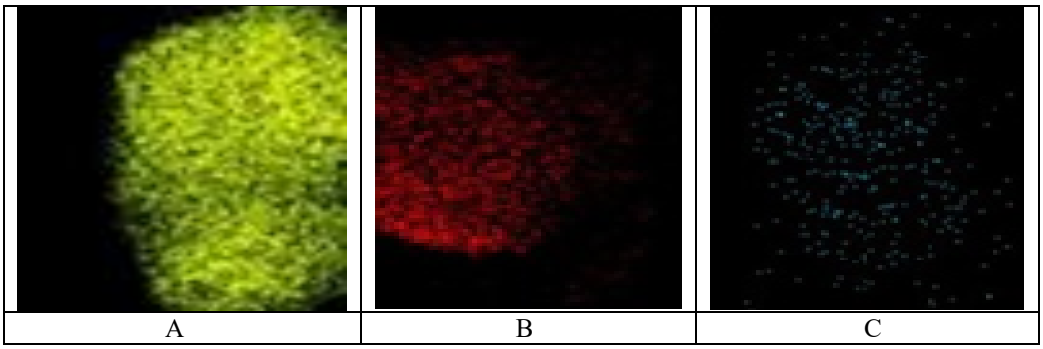

Fig. 2. STEM (HAADF) elemental mapping of $Ti_{0.95}Zr_{0.05}$ (300) after photocatalysis: (A) Ti, (B) O, (C) Cu.

The fundamental physicochemical characteristics of $Ti_{0.95}Zr_{0.05}$ (300) before and after photoreduction are presented in Fig. 3. The XRD pattern (Fig. 3A) shows that all diffraction peaks correspond to the anatase phase (PDF#21-1272), with no detectable reflections from Zr species. After photoreduction, an additional peak assigned to grimaldiite-3R (CrOOH, PDF#09-0331) appeared, indicating the formation of a Cr(VI) reduction product. No Cu-related peaks were detected, suggesting its presence only in trace amounts.

The UV–vis DRS spectra (Fig. 3B) revealed that the absorption edge of $Ti_{0.95}Zr_{0.05}$(300) remained at 380 nm with an estimated band gap (E_9) of 3.26 eV, while a new absorption band at 608 nm appeared, characteristic of Cr(III) species [,23]. This confirms the reduction and immobilization of Cr(VI) on the photocatalyst surface.

Photoreduction, distinct Cr 2p peaks at 577.4 eV and 586.8 eV emerged (Fig. 3C), corresponding to Cr(III)–OH interactions [24,25]. These results further confirm that Cr(VI) was converted to Cr(III), forming surface-bound grimaldiite species on $Ti_{0.95}Zr_{0.05}$ (300).

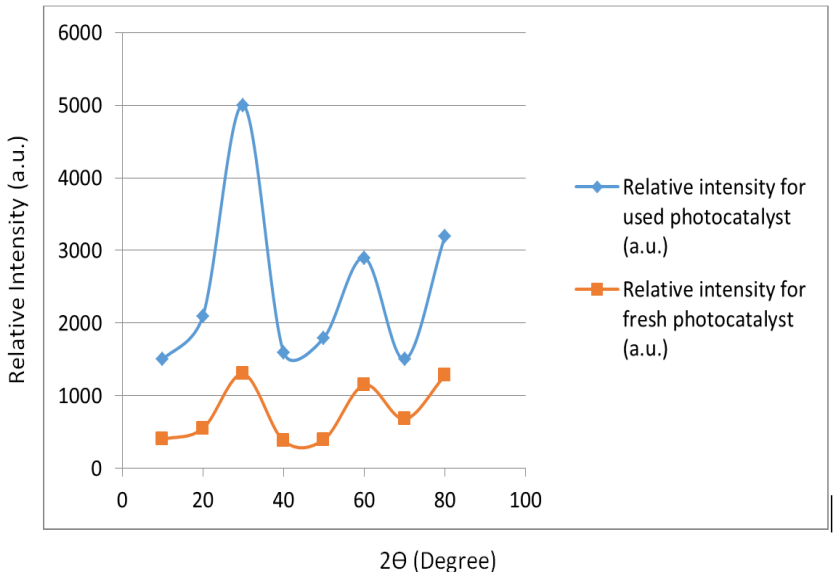
6000
5000
4000
3000
2000
1000
0
Relative Intensity (a.u.)
0
20
40
60
80
100
2Θ (Degree)
Relative intensity for used photocatalyst (a.u.)
Relative intensity for fresh photocatalyst (a.u.)

A

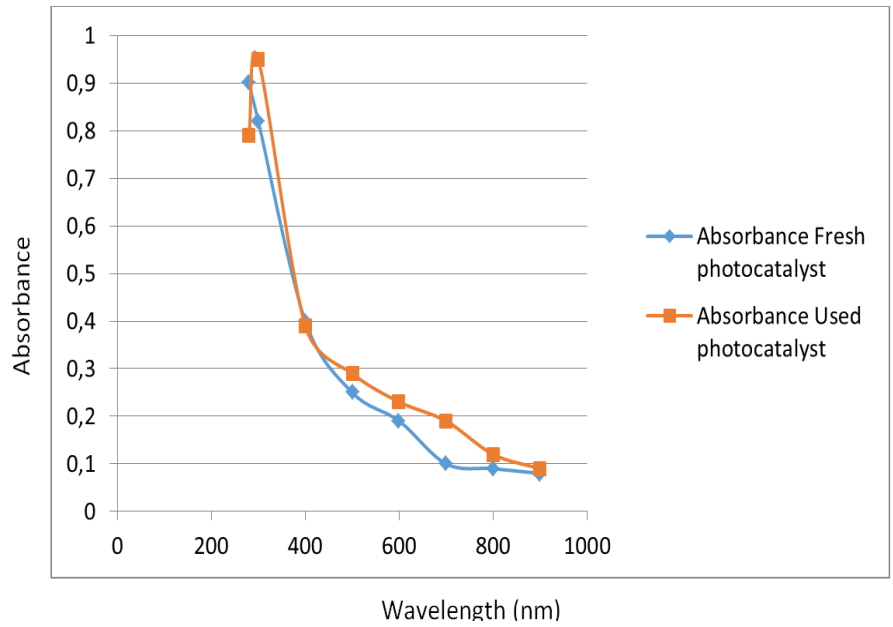
1
0,9
0,8
0,7
0,6
0,5
0,4
0,3
0,2
0,1
0
Absorbance
0
200
400
600
800
1000
Wavelength (nm)
Absorbance Fresh photocatalyst
Absorbance Used photocatalyst

B

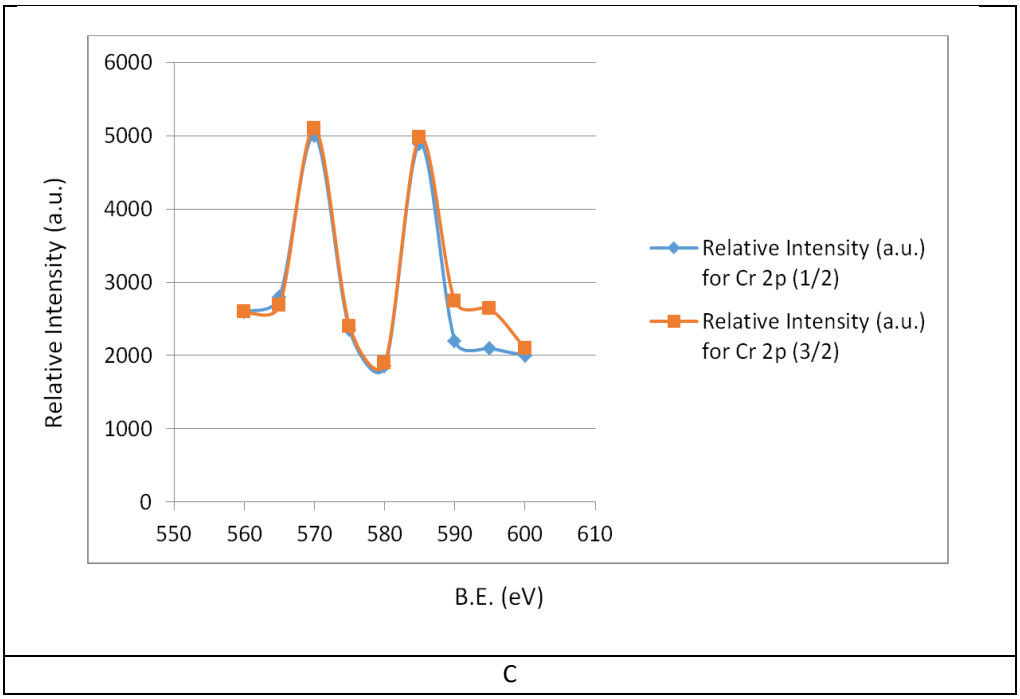

Fig. 3. Physicochemical properties of $Ti_{0.95}Zr_{0.05}$ (300) before and after photoreduction: (A) XRD patterns; (B) UV–vis DRS spectra; (C) Cr 2p spectrum of the used catalyst.

The valence band potential (E_VB) of $Ti_{0.95}Zr_{0.05}$ (300) was determined to be 2.86 eV from the XPS valence band spectrum. The conduction band potential (E_CB) was calculated to be −0.40 eV using the relation E_g = E_VB − E_CB. Based on the band structure of $Ti_{0.95}Zr_{0.05}$ (300) and the calculated redox potentials of three reducible species under acidic conditions (H^+, Cu^{2+}, and $Cr_2O_7^{2-}$), as determined by Eqs. (1)–(3) [26], $Cr_2O_7^{2-}$ was predicted to undergo preferential photoreduction by the photogenerated electrons (Fig. 4).
The calculated redox potentials were +0.83 V for $Cr_2O_7^{2-}$, +0.24 V for Cu^{2+}, and −0.18 V for H^+
1) Cr2O72−+14H++6e−⇌2Cr3++7H2O,
E=1.33+0.05916log [Cr3+]2[H+]14[Cr2O72−]V
2) Cu2++2e−⇌Cu(s),E=0.34+0.0295log[Cu2+]V
3) 2H++2e−⇌H2(g),E=0.00+0.0591log[H+]V

These results indicate that $Ti_{0.95}Zr_{0.05}$(300) selectively drives the photoreduction of $Cr_2O_7^{2-}$ over Cu^{2+} and H^+ under acidic conditions.

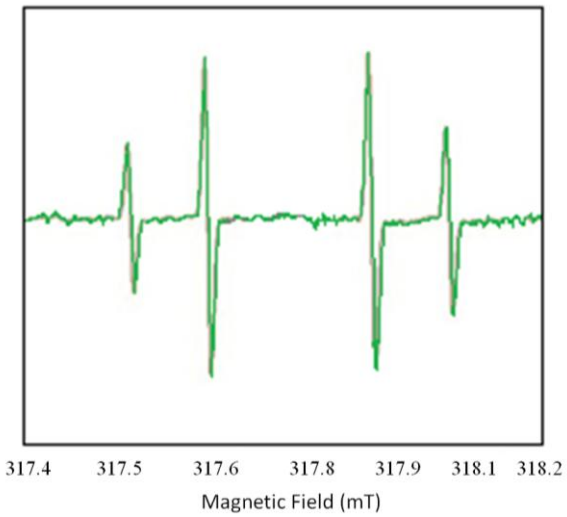

Fig. 4. Energy band structure and photoreduction mechanism of $Ti_{0.95}Zr_{0.05}$ (300): ESR analysis of reactive species.

A photo-oxidation half-reaction is inevitably required to sustain photoreduction by consuming the photo-generated holes, with H_2O acting as the primary hole scavenger. A proposed water-mediated oxidation process is as follows:

(4) $H_2O+h^+ \rightarrow \cdot OH+H^+$

(5) $2\cdot OH \rightarrow H_2O_2$

(6) $H_2O_2+h^+ \rightarrow \cdot HO_2+H^+$

(7) $Cu^+ + H_2O_2 \rightarrow \cdot OH + Cu^{2+} + OH^-$

(8) $Cu^{2+} + H_2O_2 \rightarrow Cu^+ + H^+ + \cdot HO_2$

Upon light irradiation, Ti–O and Ti–OH species form on the $Ti_{0.95}Zr_{0.05}(300)$ surface via photo-generated holes and revert to Ti–O–Ti upon release of ·OH radicals, which were detected by ESR spectroscopy (Fig. 4) [27–29]. The generated ·OH radicals are unstable and dimerize to form H_2O_2 (Eq. (5)) [29]. H_2O_2 can either be oxidized by holes (Eq. (6)) or participate in Fenton-like reactions with Cu(II) (Eqs. (7)–(8)) [30,31].

Consequently, Cu(II) cannot be reduced to Cu(0) in the absence of an external hole scavenger, even after complete Cr(VI) reduction.

This reaction pathway is indirectly supported by two observations. First, adding a hole scavenger (e.g., methanol or formic acid) to the residual hybrid solution after Cr(VI) removal enables complete Cu(II) photoreduction within 2 h. Second, the photocatalyst surface turns from white to grey during Cu(II) photoreduction, similar to $Ti_{0.95}Zr_{0.05}(300)$ in water upon H_2O_2 addition [32]. The color fades after centrifugation, attributed to auto-decomposition of adsorbed H_2O_2 on the transition metal oxides [33]

Under UV illumination, electrons are excited from the valence band to the conduction band, reducing $Cr_2O_7^{2-}$ to Cr(III) as grimaldiite. Meanwhile, holes are consumed by water to form H_2O_2, inducing Fenton-like reactions with Cu(II). Consequently, Cu(II) remains in solution and is selectively separated from the immobilized Cr species in the absence of a scavenger.

3.3. Batch studies of Cu(II) adsorption via ion-exchange with TP207

Optimization showed that TP207 completely removes Cu(II) from a pure solution without adsorbing Cr(VI). Accordingly, an adsorbent dosage of 1.0 g/L was used. As shown in Fig. 5, all Cu(II) ions in 20 mL of a 20 mg/L solution were removed within 4 h, accompanied by a color change of TP207 from beige to blue. The PFO model showed better agreement with experimental data, indicating that Cu(II) adsorption is mass-transfer controlled. The theoretical Q_{max} predicted by PFO was 20.92 mg/g, closely matching the experimental value of 20.51 mg/g, confirming that TP207 adsorption follows pseudo-first-order kinetics.

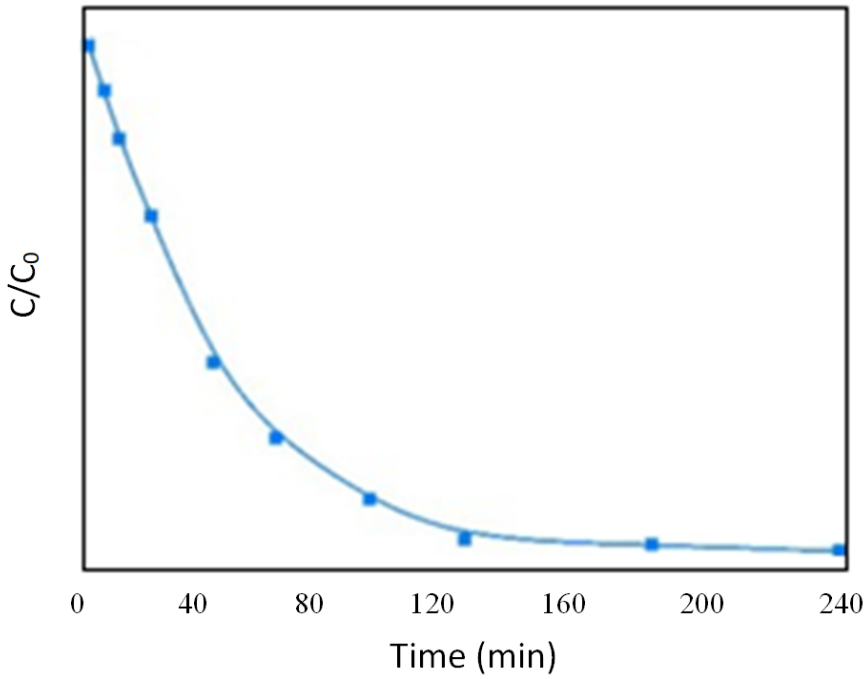

Fig. 5. Cu(II) adsorption by TP207 in simulated wastewater: Adsorption profile;

The Boyd model provided the best fit ($R^2 > 0.98$), indicating that external diffusion is the rate-limiting step controlling the overall adsorption process (Table 2). [34–36].

Table (2). Kinetic parameters for Cu(II) adsorption on Lewatit TP207 in pure Cu(II) and Cr(VI)/Cu(II) hybrid solutions (pH = 3).

Model	Parameter	Cu	Cu-Cr
PFO	Qmax (mg/g)	20.92	20.88
	Kf	0.02286	0.02165
	R^2	0.997	0.9997
PSO	Qmax (mg/g)	25.72	25.76
	Ks	9.08×10^{-4}	8.60×10^{-4}
	R^2	0.9839	0.9937
Boyd	Kfd	0.01144	0.0100
	R^2	0.9860	0.9950
Bangham	A	−3.413	−3.376
	B	0.6357	0.6083
	R^2	0.9094	0.9285
Dumwald–Wagner	K	0.0210	0.0179
	R^2	0.9687	0.9634

The presence of Cr(VI) had negligible effect on Cu(II) removal, with complete adsorption achieved within 4 h while Cr(VI) concentration remained constant. The adsorption kinetics still followed pseudo first-order behavior and the Boyd model. Slight decreases in Kf and Kfd values for the hybrid solution (Table 2) were attributed to the presence of Cr(VI).

3.4. Characterization and mechanism of Cu(II) adsorption using TP207

XPS analysis of TP207 before and after Cu(II) adsorption from the hybrid solution is shown in Fig. 6. A new Cu 2p peak appeared on the used resin, while the intensities of Na 1s and Na Auger peaks decreased, confirming ion exchange between Na^+ and Cu^{2+}. No Cr signals were detected, indicating the selective adsorption of Cu(II) by TP207.

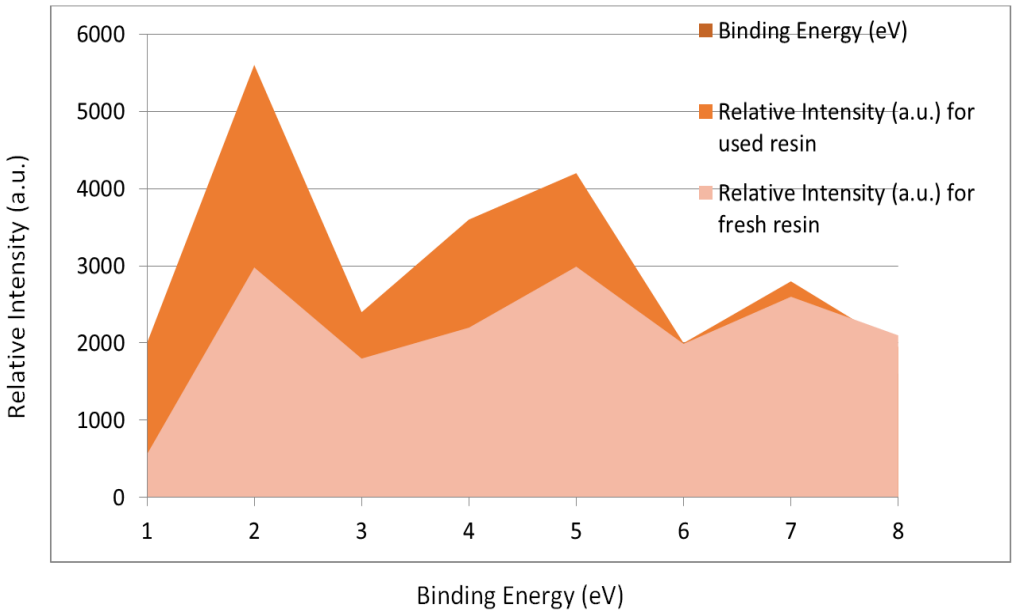

Fig. 6. Energy band structure and photoreduction mechanism of $Ti_{0.95}Zr_{0.05}$ (300): (A) XPS valence-band spectrum

After adsorption, a new peak at 532.74 eV emerged, attributable to –COOH interacting with Cu^{2+} [37,39], and the C=O/–COOH area ratio increased from 2.12 to 3.59. These observations affirm that ion exchange between Cu(II) and Na^+ in the –COONa groups of TP207 has occurred.

3.5. Column testing of Lewatit TP207 for Cu(II) removal

Column experiments were conducted to assess the performance of TP207 for Cu(II) removal under dynamic flow conditions. A glass column (7 mm inner diameter) was packed with 1.8 g of TP207 resin, and simulated Cu(II)-containing wastewater was pumped from the top at a flow rate of 8.0 mL min^{-1}. Breakthrough curves were generated by monitoring the effluent Cu concentration over time.

The results showed that TP207 effectively removed Cu(II) until the onset of breakthrough; beyond this point the effluent concentration rose sharply. The resin maintained high removal efficiency until a significant fraction of its exchange sites were exhausted. These outcomes verify that TP207 in a fixed-bed column configuration is capable of continuous Cu(II) removal and that its dynamic capacity and kinetics are consistent with the batch adsorption behaviour previously observed.

If you like, I can format the breakthrough-curve data including bed volumes, breakthrough time, and exhaustion time into a tabular form and provide recommended column design parameters (e.g., bed height, flow rate, resin mass) for scale-up.

IV. CONCLUSION

This study demonstrated the effective removal and recovery of Cu(II) and Cr(VI) ions from metal industry wastewater using a nanocomposite-based treatment approach. The synthesized nanocomposite exhibited high adsorption capacity and strong affinity toward both metal ions, highlighting its potential as an efficient and versatile adsorbent for wastewater remediation. The adsorption performance was significantly influenced by key operational parameters such as pH, contact time, initial metal ion concentration, and adsorbent dosage, with optimal conditions resulting in maximum removal efficiencies.

The adsorption behavior of Cu(II) and Cr(VI) was well described by established isotherm and kinetic models, indicating favorable adsorption mechanisms and rapid uptake. Moreover, the nanocomposite demonstrated good regeneration and reusability through successive adsorption–desorption cycles, confirming its stability and economic feasibility for repeated use. The successful recovery of metal ions further emphasizes the potential of this method not only for environmental protection but also for resource recovery.

Overall, the findings suggest that the proposed nanocomposite is a promising candidate for the treatment of metal-laden industrial wastewater. Its high efficiency, reusability, and capability for metal recovery make it suitable for sustainable and cost-effective wastewater management. Future research should focus on large-scale applications, long-term performance evaluation, and the treatment of real industrial effluents to further validate its practical applicability.

[1]. Y. Feng, S.M. Yang, L. Xia, Z.W. Wang, N. Suo, H. Chen, Y.Y. Long, B. Zhou, Y.Z. Yu In-situ ion exchange electrocatalysis biological coupling (i-IEEBC) for simultaneously enhanced degradation of organic pollutants and heavy metals in electroplating wastewater J. Hazard. Mater., 364 (2019), pp. 562-570

[2]. Y.Y. Gong, J.C. Tang, D.Y. Zhao.,Application of iron sulfide particles for groundwater and soil remediation: A review.Water Res., 89 (2016), pp. 309-320

[3]. X. Zhao, L.B. Guo, B.F. Zhang, H.J. Liu, J.H. Qu.,Photoelectrocatalytic oxidation of Cu^{II}-EDTA at the TiO_2 electrode and simultaneous recovery of Cu^{II} by electrodeposition Environ. Sci. Technol., 47 (2013), pp. 4480-4488

[4]. P. Rudnicki, Z. Hubicki, D. Kołodynska.,Evaluation of heavy metal ions removal from acidic waste water streams. Chem. Eng. J., 252 (2014), pp. 362-373

[5]. O. Fellahi, A. Barras, G.H. Pan, Y. Coffinier, T. Hadjersi, M. Maamache, S. Szunerits, R. Boukherroub.Reduction of Cr(VI) to Cr(III) using silicon nanowire arrays under visible light irradiation ,J. Hazard. Mater., 304 (2016), pp. 441-447

[6]. S. Satyro, R. Marotta, L. Clarizia, I.D. Somma, G. Vitiello, M. Dezotti, G. Pinto, R.F. Dantas, R. Andreozzi, Removal of EDDS and copper from waters by TiO_2 photocatalysis under simulated UV-solar conditions Chem. Eng. J., 251 (2014), pp. 257-268

[7]. W.Q. Cai, L.J. Tan, J.G. Yu, M. Jaroniec, X.Q. Liu, B. Cheng, F. Verpoort.,Synthesis of amino-functionalized mesoporous alumina with enhanced affinity towards Cr(VI) and CO_2 Chem. Eng. J., 239 (2014), pp. 207-215

[8]. L. Luo, W.Q. Cai, J.B. Zhou, Y.Z. Li Facile synthesis of boehmite/PVA composite membrane with enhanced adsorption performance towards Cr(VI), J. Hazard. Mater., 318 (2016), pp. 452-459

[9]. A. Janin, J.F. Blais, G. Mercier, P. Drogui,Selective recovery of Cr and Cu in leachate from chromated copper arsenate treated wood using chelating and acidic ion exchange resins, J. Hazard. Mater., 169 (2009), pp. 1099-1105

[10]. W.Q. Cai, Z.L. Li, J.H. Wei, Y. LiuSynthesis of peanut shell based magnetic activated carbon with excellent adsorption performance towards electroplating wastewater,Chem. Eng. Res. Des., 140 (2018), pp. 23-32

[11]. W.Q. Cai, M.M. Gu, W. Jin, J.B. Zhou,CTAB-functionalized C@SiO_2 double-shelled hollow microspheres with enhanced and selective adsorption performance for Cr(VI), J. Alloy. Compos., 777 (2019), pp. 1304-1312

[12]. N. Aman, T. Mishra, J. Hait, R.K. Jana,Simultaneous photoreductive removal of copper (II) and selenium (IV) under visible light over spherical binary oxide photocatalyst, J. Hazard. Mater., 186 (2011), pp. 360-366

[13]. N. Li, Y. Tian, J.H. Zhao, J. Zhang, J. Zhang, W. Zuo, Y. Ding,Efficient removal of chromium from water by Mn_3O_4@ZnO/Mn_3O_4 composite under simulated sunlight irradiation: Synergy of photocatalytic reduction and adsorption. Appl. Catal. B-Environ., 214 (2017), pp. 126-136

[14]. Z.P. Chen, Y.R. Li, M. Guo, F.Y. Xu, P. Wang, Y. Du, P. Na,One-pot synthesis of Mn-doped TiO_2 grown on graphene and the mechanism for removal of Cr(VI) and Cr(III).J. Hazard. Mater., 310 (2016), pp. 188-198

[15]. K. Kabra, R. Chaudhar, R.L. Sawhney,Treatment of hazardous organic and inorganic compounds through aqueous-phase photocatalysis: A review.Ind. Eng. Chem. Res., 43 (2004), pp. 7683-7696

[16]. X. Zhao, L.B. Guo, C.Z. Hu, H.J. Liu, J.H. Qu,Simultaneous destruction of Nickel (II)-EDTA with TiO_2/Ti film anode and electrodeposition of nickel ions on the cathode.Appl. Catal. B-Environ., 144 (2014), pp. 478-485

[17]. W. Jiang, Q. Liu, Y. Tao, K.Q. Mu, Z. Wang, Y.M. Zhu, H.R. Yue, B. Liang,.,An environment-friendly strategy for one-step turning Cr(VI) contaminant into a Cr-loaded catalyst for CO_2 utilization.Adv. Sustain. Syst., 2 (2018), p. 1700165

[18]. Y.S. Liu, S.H. Wei, W. Gao.,Ag/ZnO heterostructures and their photocatalytic activity under visible light: Effect of reducing medium.,J. Hazard. Mater., 287 (2015), pp. 59-68

[19]. Y. Guo, L. Zhang, K.L. Zhou, Y. Shen, Q.J. Zhang, C. Gu.Selective gold recovery by carbon nitride through photoreduction.,J. Mater. Chem. A, 2 (2014), pp. 19594-19597

[20]. W. Liu, J.R. Ni, X.C. Yin.Synergy of photocatalysis and adsorption for simultaneous removal of Cr(VI) and Cr(III) with TiO_2 and titanate nanotubes.,Water Res., 53 (2014), pp. 12-25

[21]. G.G. Zhang, Z.A. Lan, L.H. Lin, S. Lin, X.C. Wang.,Overall water splitting by Pt/g-C_3N_4 photocatalysts without using sacrificial agents,Chem. Sci., 7 (2016), pp. 3062-3066

[22]. J. Zhang, N. Gao, F.L. Chen, T. Zhang, G.L. Zhang, D.F. Wang, X.Y. Xie, D.Q. Cai, X.J. Ma, L.F. Wu, Z.Y. Wu.,Improvement of Cr (VI) photoreduction under visible-light by g-C_3N_4 modified by nano-network structured palygorskite.Chem. Eng. J., 358 (2019), pp. 398-407

[23]. A. Węgrzyniak, A. Rokicińska, E. Hędrzak, B. Michorczyk, K. Zeńczak-Tomera, P. Kuśtrowski, P. Michorczyk.,High-performance Cr–Zr–O and Cr–Zr–K–O catalysts prepared by nanocasting for dehydrogenation of propane to propene,Catal. Sci. Technol., 7 (2017), pp. 6059-6068

[24]. S.Q. Guo, L.N. Xu, L. Zhang, W. Chang, M.X. Lu.,Corrosion of alloy steels containing 2% chromium in CO_2 environments,Corros. Sci., 63 (2012), pp. 246-258

[25]. E. Desimoili, C. Malitesta, P.G. Zambonin, J.C. Riviere.,An X-ray photoelectron spectroscopic study of some chromium-oxygen systems,Surf. Interface Anal., 13 (1988), pp. 173-179

[26]. A.J. Bard.,Standard potentials in aqueous solution,(1st ed.), M. Dekker, New York, New York (1985)

[27]. Y. Nosaka, A.Y. Nosaka.,Generation and detection of reactive oxygen species in photocatalysis,Chem. Rev., 117 (2017), pp. 11302-11336

[28]. J. Zhang, Y. Nosaka.,Photocatalytic oxidation mechanism of methanol and the other reactants in irradiated TiO_2 aqueous suspension investigated by OH radical detection,Appl. Catal. B-Environ., 166–167 (2015), pp. 32-36

[29]. W. Kim, T. Tachikawa, G.H. Moon, T. Majima, W. Choi.,Molecular-level understanding of the photocatalytic activity difference between anatase and rutile nanoparticles,Angew. Chem. Int. Edit., 53 (2014), pp. 14036-14041

[30]. L. Zhang, B.D. Wu, G.Y. Zhang, Y.H. Gan, S.J. Zhang.,Enhanced decomplexation of Cu(II)-EDTA: The role of acetylacetone in Cu-mediated photo-Fenton reactions Chem. Eng. J., 358 (2019), pp. 1218-1226

[31]. K. Sahel, L. Elsellami, I. Mirali, F. Dappozze, M. Bouhent, C. Guillard.,Hydrogen peroxide and photocatalysis,Appl. Catal. B-Environ., 188 (2016), pp. 106-112

[32]. C.M. Lousada, A.J. Johansson, T. Brinck, M. Jonsson.,Mechanism of H_2O_2 decomposition on transition metal oxide surfaces, J. Phys. Chem. C, 116 (2012), pp. 9533-9543

[33]. J. Acharya, J.N. Sahu, C.R. Mohanty, B.C. Meikap.,Removal of lead(II) from wastewater by activated carbon developed from Tamarind wood by zinc chloride activation,Chem. Eng. J., 149 (2009), pp. 249-262

[34]. J. Acharya, J.N. Sahu, B.K. Sahoo, C.R. Mohanty, B.C. Meikap.,Removal of chromium(VI) from wastewater by activated carbon developed from Tamarind wood activated with zinc chloride, Chem. Eng. J., 150 (2009), pp. 25-39

[35]. R. Aravindhan, J.R. Rao, B.U. Nair.,Removal of basic yellow dye from aqueous solution by sorption on green alga Caulerpa scalpelliformis, J. Hazard. Mater., 142 (2007), pp. 68-76

[36]. J.A. RamosGuivar, E.A. Sanches, F. Bruns, E. Sadrollahi, M.A. Morales, E.O. López, F.J. Litterst., Vacancy ordered γ-Fe_2O_3 nanoparticles functionalized with nanohydroxyapatite: XRD, FTIR, TEM, XPS and Mössbauer studies, Appl. Surf. Sci., 389 (2016), pp. 721-734

[37]. J.C. Yu, F.G. Zhao, W. Shao, C.W. Ge, W.S. Li.,Shape-controllable and versatile synthesis of copper nanocrystals with amino acids as capping agents, Nanoscale, 7 (2015), pp. 8811-8818

[38]. X.C. Yin, J. Long, Y. Xi, X.B. Luo.,Recovery of silver from wastewater using a new magnetic photocatalytic ion-imprinted polymer,ACS Sustain. Chem. Eng., 5 (2017), pp. 2090-2097

[39]. Y.X. Zhang, M.J. Xu, H. Li, H. Ge, Z.F. Bian., The enhanced photoreduction of Cr(VI) to Cr(III) using carbon dots coupled TiO_2 mesocrystals,Appl. Catal. B-Environ., 226 (2018), pp. 213-219